International Journal of Bridge Engineering (IJBE), Special Issue 2016, pp. 197-219

BRIDGE SUBJECTED TO SURFACE FAULT RUPTURE
Part I: Numerical Investigation

Antonios Kladis[1], Fani Gelagoti[2], Marianna Loli[3] and George Gazetas[4]

[1,2,3,4] National Technical University of Athens, Deptartment of Civil Engineering, Greece
e-mail: anthony.kladis@gmail.com, fanigelagoti@gmail.com, mariannaloli@yahoo.com, gazetas@central.ntua.gr

ABSTRACT: Surface fault ruptures may inflict serious damage to bridges built on top or near them, as amply demonstrated in three notorious earthquakes, Kocaeli, Chi–Chi, and Wenchuan, among others. Successes have also been observed, providing the impetus for research into the design against tectonic deformation. To circumvent the formidable 3D analysis, previous research efforts on the subject had decomposed the problem, with the free-field solution of the fault propagation as a first step, followed by the analysis of the bridge system subjected to the calculated deformations of the free-field step. This paper attempts a robust investigation of the entire bridge system (soil, foundation, pier, deck) with the intention to elucidate the significance (or not) of the kinematic constraints imposed by the superstructure on the overall bridge response. To this end, a typical highway bridge founded on shallow footings is subjected to a dip–slip "normal" and "thrust" faulting. A series of physical model-scale experiments are about to be conducted in a split-box apparatus, capable of imposing normal and thrust type base offsets. In this study (before the model tests are conducted) a numerical prediction of the forthcoming experimental results is attempted, evaluating simultaneously the decoupled methodology of *Anastasopoulos et al. 2008*. 2D finite element analyses accounting for soil strain-softening are conducted. The position of the footing relative to the surface fault rupture and the imposed kinematic constraints on the abutments are also parametrically investigated, assessing the developing various mechanisms and the corresponding distress of the bridge. This paper is the first of a two-paper sequence presenting a genuine numerical prediction of a forthcoming physical experiment at a 1:15 scale.

KEYWORDS: Normal fault, thrust fault, soil–foundation–bridge interaction.

INTRODUCTION

In some earthquakes the seismogenic fault ruptures all the way to the ground surface. This is particularly frequent with larger magnitude (M > 6.5) events and in the case of dip-slip faults it produces one or more scarps on the ground

surface. A large scale of ground subsidence (if the fault is "normal") or upheaval (if the fault is "thrust") is the result of the moving block (the so-called "hanging-wall") being displaced. The rupture emerges slowly (as a quasi-static displacement) starting from the bedrock, propagating within the soil deposit, emerging on the ground surface, and hence subjecting any structure on its path to extreme differential placements often leading to collapse or excessive tilting.

Survival however is not impossible. Structures, if designed appropriately, may withstand major fault offsets, thanks to the favorable interplay of the rupture with the soil and foundation [*Bray JD. 2001, 2009; Fadaee et al. 2013; Gazetas et al. 2008, 2015*]. The mechanics of such interaction have been explored by many researchers [*Oettle & Bray, 2013; Bray & Seed, 1994; Anastasopoulos et al. 2008, 2009; Loli et al. 2011*], suggesting that fault rupture may be "forced" to deviate due to the presence of the structure, protecting it from unfavorable tectonic deformations. Rigid and continuous foundations of high surcharge were found to perform best, especially if founded on soft / loose soil.

2 SCOPE OF THIS STUDY

This paper investigates the response of a bridge system crossed by an emerging fault. Previous studies on the subject propose the use of a two-step decoupled methodology [*Anastasopoulos et al. 2008*]. In the first step the response of a single bridge pier subjected to fault rupture deformation is analyzed, while in the second the detailed model of the superstructure is subjected to the computed, from the previous step, displacements. In other words it has been assumed that the superstructural system does not affect the soil and bridge footing deformations. The validity of this assumption will be checked herein by comparing the response of a coupled soil-fault-foundation-bridge system with the response assessed by applying the decoupled methodology of *Anastasopoulos et al. 2008.*

The problem is studied both numerically and experimentally and the results are presented in a set of two papers. In this first paper, the numerically methodology is briefly outlined and a class-A prediction of the 1-g experiments is attempted. The experiments are being conducted in the Fault Rupture Box (FRB) of the NTUA [*Gazetas et al. 2015*], assuming a model scale of 1:15. The dimensions and material properties of the model were scaled down employing appropriate similarity laws [*Muir Wood. 2004*]. The results of the experiments will be presented in a second (companion) paper.

The structural system of the bridge (i.e. the pier-deck connections and the boundary conditions at the abutments), as well as the fault outcropping position are parametrically investigated. For the sake of brevity, results are presented for the most unfavorable case: the pier is monolithically connected to the deck, and the fault crosses the foundation of the central pier.

3 PROBLEM STATEMENT

The investigated model is from an actual (and typical) two-span highway bridge with total length of 34.5 m (Fig. 1). The deck is a hollow section made of pre-stressed concrete, with effective section area of 4.96 m^2 and inertia moment 0.81 m^4. The deck supports a rectangular 8 m high concrete pier, with dimensions in plan 0.9 x 3.8 m. The central pier is monolithically connected to the deck beams, while at each of the two abutments the deck rests on top of two elastomeric bearings.

The pier is supported on shallow footings of dimensions L = 7.5 m x B = 2.1 m on top of a sandy stratum. The soil stratum is dry sand with 60% relative density. The bedrock (lying 6 m below the ground surface) is subjected to a 45^o dip-slip angle tectonic dislocation (normal and reverse faulting).

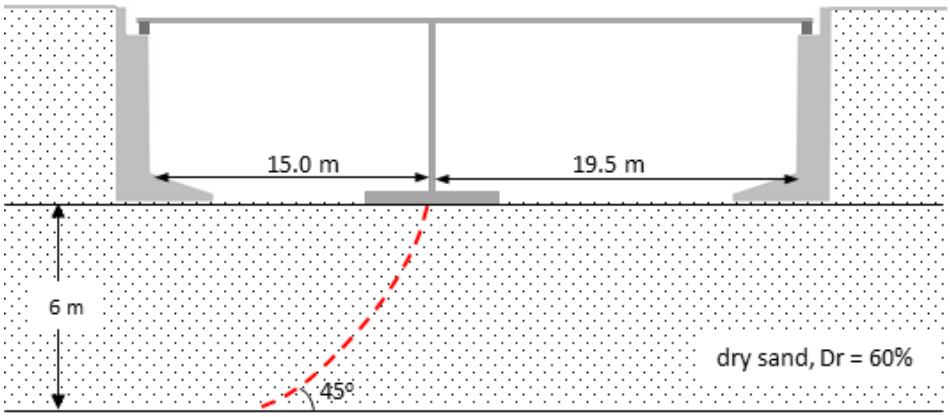

Figure 1. Sketch of the studied problem indicating the key parameters and dimensions at prototype scale. Dimensions apply to both **normal** and **thrust** rupturing faulting

4 BRIDGE SUBJECTED TO FAULTING: COUPLED VS DE-COUPLED ANALYSES

(a) Presentation of the Coupled Methodology

The finite element (FE) method has been applied successfully by several researchers to simulate the fault rupture propagation process in the free-field, as well as the interplay of fault–foundation–structure systems [*Anastasopoulos et al. 2007, 2009; Loli et al. 2011; Bray et al. 1994; Loukidis et al. 2009; Bransby et al. 2008*]. In this study, the soil–foundation-bridge system is analysed under plane strain conditions. The model (Fig. 2) is a numerical replica of the Fault Rupture Split Box experimental apparatus, and hence its dimensions are equal to those of the split-box. The depth of the soil stratum is 0.40 m (6 m in prototype), while the length is 2.60 m. Note that the length/depth ratio is greater than 4, as required to minimize any undesired boundary effect. Only prototype

dimensions are given from now on.

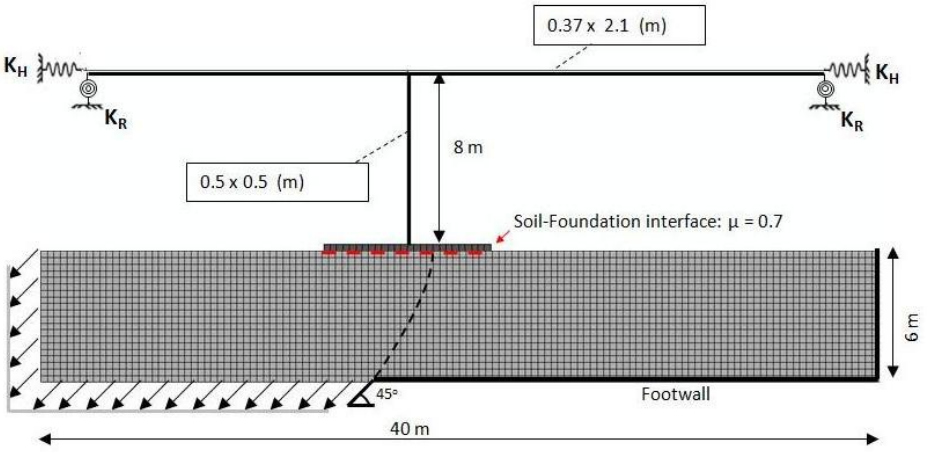

Figure 2. View of the 2D Finite Element model, along with key dimensions and boundary conditions

Soil and surface footing are simulated with 4-noded plane-strain continuum elements. Following the recommendations of Bray et al (1994), in order to properly simulate the developed shear band, the FE mesh in the neighborhood of the potential rupture should be very refined and a rigorous nonlinear constitutive law for the soil should be assumed. In our numerical model the smallest finite element size is d_{FE} = 0.3 m.

The soil is modelled employing the elastoplastic constitutive model described in [*Anastasopoulos et al. 2007*], and encoded in ABAQUS as a user-defined subroutine. The model incorporates elastic pre-yielding soil behavior, assuming a shear modulus G_S linearly increasing with depth. A Mohr–Coulomb failure criterion is combined with isotropic strain softening, reducing the friction φ and dilation ψ angles with octahedral plastic shear strain γ_{oct}^{pl} according to the following relationships:

$$\left.\begin{aligned} \varphi &= \varphi_p - \frac{\varphi_\rho - \varphi_{res}}{\gamma_f^{pl}}\,\gamma_{oct}^{pl} \\ \psi &= \psi_p\left(1 - \frac{\gamma_{oct}^{pl}}{\gamma_f^{pl}}\right) \end{aligned}\right\} \quad \text{for} \quad 0 \le \gamma_{oct}^{pl} \le \gamma_f^{pl}$$
$$\psi_{res} = 0 \qquad \text{for} \quad \gamma_{oct}^{pl} \ge \gamma_f^{pl} \tag{1}$$

Where φ_p and φ_{res} the peak and residual soil friction angles; ψ_p the peak dilation angle; and γ_f^{pl} the octahedral plastic shear strain at the end of softening. Constitutive soil parameters are calibrated on the basis of direct shear tests. This

model has been adequately validated against centrifuge experiments conducted at the University of Dundee by Bransby et al, 2008, as discussed in detail in *Anastasopoulos et al. 2007*.

For the small stresses of the reduced-scale experiments presented herein, the mobilized friction angle depends strongly on the stress level. This problem, which does not exist in the centrifuge models where the stress level is equivalent to prototype reality, is known as *scale effects*. To account for such effects in the numerical modelling, φ and ψ are being iteratively adjusted (according to Eq. 1) to be always consistent with γ_f^{pl} and σ_{oct} (octahedral stress).

The fault offset is simulated as a monotonically increasing displacement at the model base. The bottom boundary is divided into two parts; one part (right) remains stationary (representing the so-called "footwall"), and the other (left) block moves up or down to simulate normal or reverse faulting, respectively. After imposing the geostatic stresses and the dead load of the superstructure, the fault dislocation is applied in small quasi-static analysis increments.

The pier and the deck are modeled with 2-noded beam elements, while the bearings of each abutment are modelled using special 2-noded elastic spring elements of horizontal stiffness K_H = 3846 kN/m and rotational stiffness K_R = 22222 kNm/rad. The vertical stiffness of the abutments is very high and therefore zero vertical displacement has been prescribed.

The soil-footing interface is modelled using special contact elements that allow sliding, uplifting and separation (loss of contact). In the experiments, sandpaper are glued on the bottom of footing to increase the interface friction to realistic levels. Thus, a friction coefficient of $\mu = 0.7$ is an appropriate value for the interface between sand and sandpaper.

The bridge deck is modeled as linearly elastic expecting the bending moments to be much lower than the bending capacity of this massive deck). The pier, on the other hand is simulated assuming the moment (**M**)–curvature (**1/r**) relation plotted in Fig. 3. The ultimate value of pier moment is M_{ult} = 6500 kNm.

The backfill of the experiment will consist of dry ''Longstone'' sand, a very fine uniform quartz sand with d_{50} = 0.15 mm and uniformity coefficient $C_u = D_{60}/D_{10} \approx 1.4$, industrially produced with adequate quality control. The void ratios at the loosest and densest state have been measured as e_{max} = 0.995 and e_{min} = 0.614, while G_s = 2.64. Direct shear tests have been carried out to obtain the peak and post-peak strength characteristics of the sand. Medium loose [D_r = (45 ± 2 %)] and dense [D_r = (80 ± 3 %)] sand specimens were tested at normal stresses ranging from 13 kPa (due to the weight of the top cap only) to 300kPa, while the correspondent soil data for medium dense sand [D_r = (60 ± 2 %)] was deduced using linear interpolation.

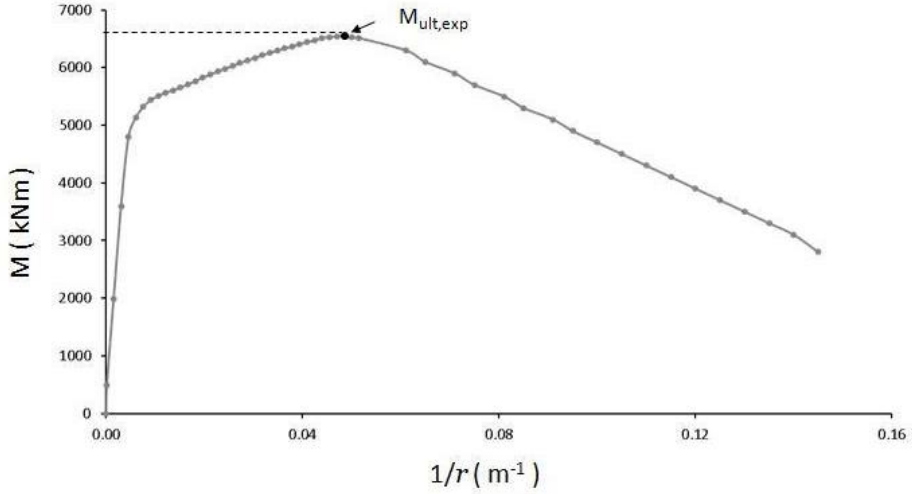

Figure 3. The Non-linear Bending response of the RC bridge pier (prototype scale), in terms of curvature ($1/r$) – moment (M)

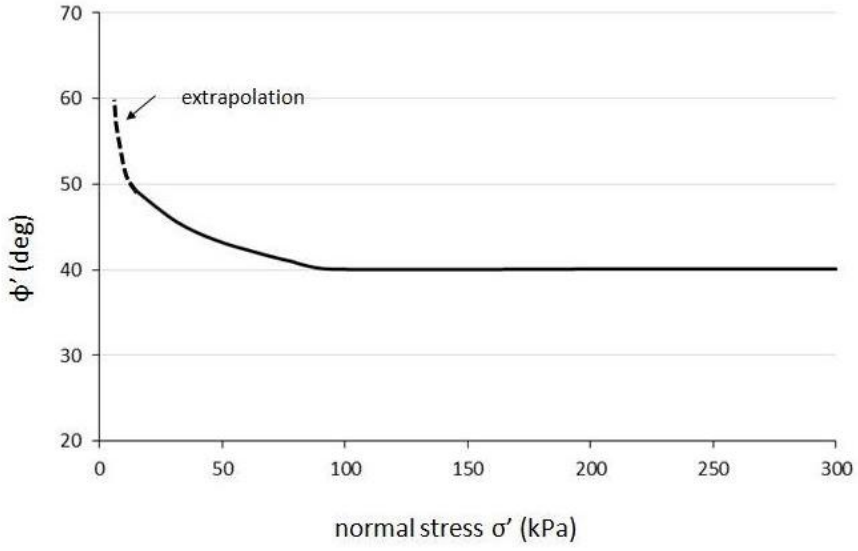

Figure 4. Direct shear results for the Longstone sand: mobilized friction angle as a function of stress level

As documented in *Anastasopoulos et al. 2010*, the angle of shearing resistance depends strongly on the stress level; for stresses higher than 120 kPa, referring to loose sand, $\varphi' = 32^o$ while for lower stresses φ' increases up to 45^o. For the dense specimens the angle of shearing resistance is 35^o for the higher stress levels and 51^o at the lowest normal stress tested. For the soil of this study [D_r =

(60 ± 2 %)], the distribution of φ' in function with specimen vertical stress (σ) is shown in Fig. 4. These values drop for displacements greater than 6 mm to post-peak critical-state. The angle of dilation also depends on the effective stress [Bolton. 1986], with a maximum value $\psi = 12^o$.

(b) The Decoupled Two-Step Methodology

To rigorously assess the performance of a structure undergoing large tectonic deformation, the analysis of the entire soil-fault-structure system is performed in a single step (Fig. 2). This type of analysis (the attributes of which were presented in previous paragraphs) is not so simple. To overcome this obstacle *Anastasopoulos et al. 2008* proposed a simplified methodology for the design of bridges against faulting.

The problem is decoupled in two consecutive analysis steps. In the first step, the response of a single pier and its foundation to fault rupture propagating through the soil is modeled (local model), while the superstructure is introduced in a simplified manner. In particular, as schematically portrayed in Fig.5, the local model should include: the soil, the foundation, and the bridge-pier (of height H_p and stiffness EI_p), while the bridge deck is replaced by equivalent lateral and rotational springs, K_x and K_θ, respectively.

For the case of a continuous deck monolithically connected to piers, K_x represents the axial stiffness of the deck and K_θ the bending stiffness of the pier-deck connection. Correspondingly, for a seismically isolated bridge, K_x and K_θ represent the lateral and rotational stiffness of the (elastomeric) bearings. In our study, the pier is monolithically connected with deck and (elastomeric) bearings are placed on the edges of model. For this reason, the axial stiffness of deck K_x is substituted with the horizontal stiffness of the bearings, while the rotational stiffness K_θ, is equal with the bending stiffness of the pier-deck connection. This step provides the horizontal (Δx) and vertical (Δy) displacements and the rotation θ at the base of pier that are necessary for the next step. In the second Step, the detailed model of the superstructure (global model) is analysed subject to the support (differential) displacements estimated in the previous step.

This paper attempts a direct comparison between the coupled and the de-coupled type of analysis for a bridge system experiencing normal or reverse faulting. The comparison will be provided in terms of settlement and rotation at bridge-footing, bending moments in the pier and the deck.

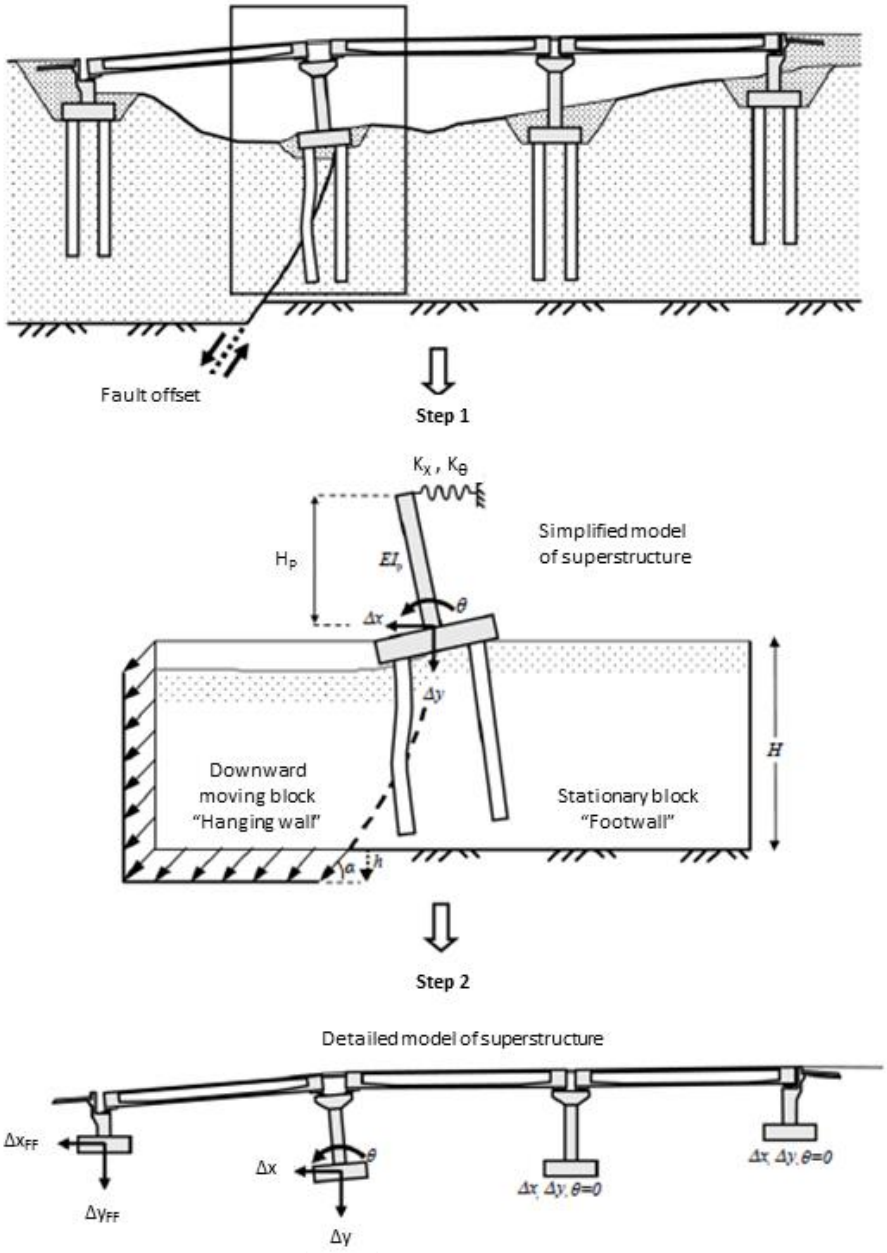

Figure 5. The decoupled Methodology of *Anastasopoulos et al (2008)*: the analysis of the soil-structure system subjected to faulting-induced deformation is conducted in two steps. In Step 1, we analyze the response of a single bridge pier subjected to fault rupture deformation. In Step 2, the detailed model of the superstructure is subjected to the computed displacements and rotations of Step 1.

5 RESULTS: BRIDGE SUBJECTED TO NORMAL FAULTING

As a first example, a normal fault rupture with an offset at bedrock (in prototype scale) of 1.5 m is imposed on the system (δ = 0.25 H). This is a large but not unusual offset value having been observed in several recent events. It is however the largest value considered here; hence $\delta = \delta_{max} = -1.5$ m (negative values are used to denote downwards, normal fault movement).

Fig. 6 portrays the propagation of the rupture within the soil stratum and the consequent footing and bridge response. Observe that while the free field fault would be expected to emerge under the footing midpoint, a double deviation takes place along with a bifurcation of the rupture line. No gap develops between footing and soil, but a substantial positive rotation (of about 0.23 rad) is unavoidable, inducing positive curvature on the pier base. The coupled system is further distressed by the imposed displacements of the left abutment. The latter displaces the top of the pier to the left introducing a negative curvature on the pier base, practically relieving the pier from the bending due to foundation rotation. Thus broader margins of safety are expected by the coupled analysis.

In Fig. 6 (b, c) response is assessed utilizing both the coupled and the decoupled methodology. Fig. 6(b) compares the bending stress for the two bridge piers. Evidently, both analyses result in a very similar pier response. Failure occurs first at the base of the pier, followed by a rapid increase of bending moment at the top section (pier-deck connection). Yet, the decoupled system fails first (at $\delta/\delta_{max} \approx 0.27$), compared to the coupled system where failure is expected for a slightly higher fault dislocation (at $\delta/\delta_{max} \approx 0.33$). The paradox in this behavior is that the onset of failure in the two piers is different, although both experience identical footing rotations.

Fig. 7(a) compares the settlement and rotation of the footing for the two types of analyses. The results are very close: the footing in both analyses responds in a quite similar manner. However, it is interesting to note the irregularity in the evolution of foundation displacements for the decoupled system at $\delta/\delta_{max} \approx 0.30$. A schematic explanation of this peculiar behavior is portrayed in Fig. 7(b). Initially (for $\delta/\delta_{max} < 0.30$), a clear gap appears at the left corner of footing as the hanging wall offset increases. This gap rapidly closes at $\delta/\delta_{max} \approx 0.33$ when a plastic hinge at the base of the pier (indicated at $\delta/\delta_{max} \approx 0.27$) has fully formed. At that instant, the superstructure abruptly (evidenced by the step-like pattern in the plots at that particular instant) follows the ground deformation being unable to resist the imposed deformation.

The differences are far more pronounced in terms of deck drift ratio, as presented in Fig. 8(a). For $\delta < 0.27\ \delta_{max}$ (i.e. before plastic hinging of the pier), both systems develop positive drift ratios as a result of the left rotation of the footing. Of course, it comes as no surprise that thereafter the drift of the coupled system is much higher. This is because fault dislocations are simultaneously felt

at bedrock (base of model) and the left abutment (lying on the hanging wall) dragging the bridge pier farther to the left, while in the decoupled system the drift results solely from bedrock dislocation.

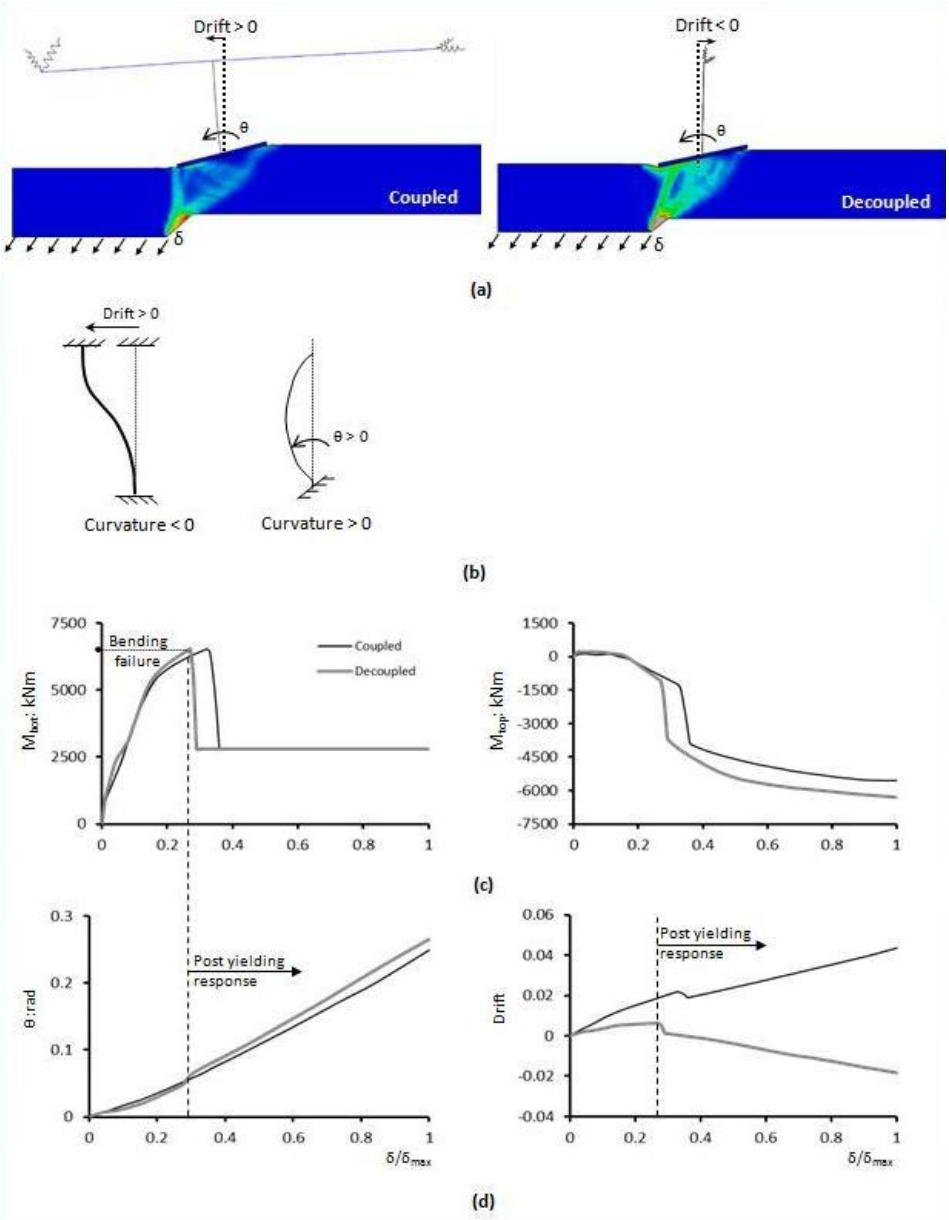

Figure 6. Bridge subjected to normal faulting ($\delta_{max} = -1.5$ m): (a) View of the deformed coupled and decoupled system; (b) kinematics responsible for the bending stressing on the pier of the coupled system. Results are presented in terms of: (c) bending moments on the top (M_{top}) and bottom (M_{bot}) of the pier; and (d) rotation of footing (θ) and drift ratio of pier

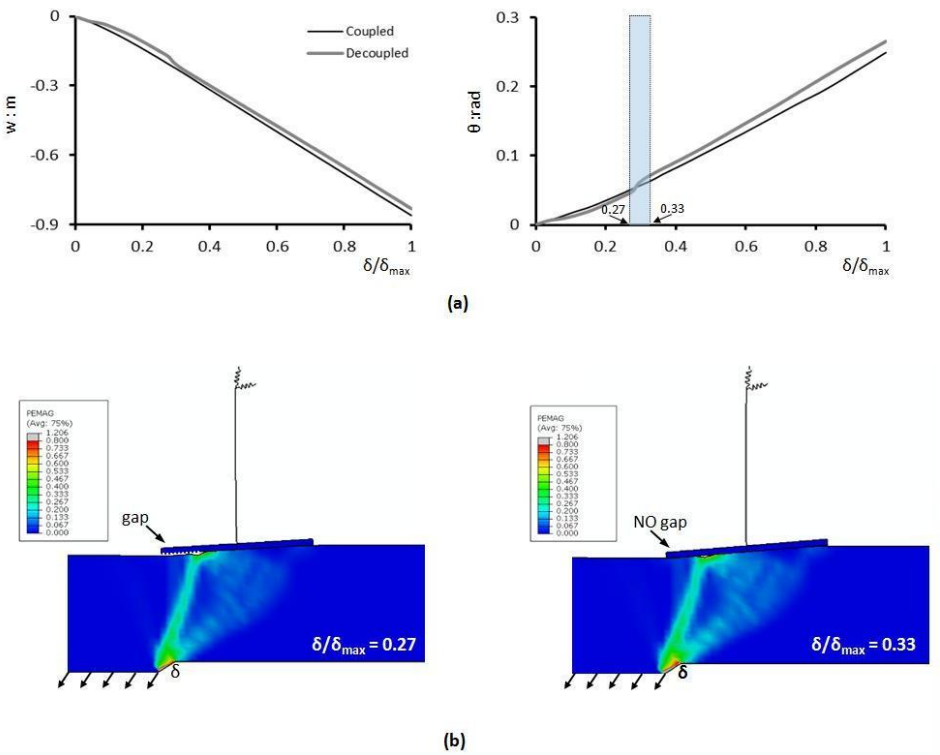

Figure 7. Bridge subjected to normal faulting ($\delta_{max} = -1.5$ m): (a) settlement (w) and rotation (θ) at the footing and (b) snapshots of the deformed decoupled problem at two distinctive instants

This trend changes completely after plastification of the pier. The coupled system keeps accumulating positive drifts while the decoupled system reverses to negative drifts. A view of the deformed mesh at time-step $\delta/\delta_{max} \approx 0.8$ is illustrated in Fig. 8(b) to assist the interpretation of this behavior. After pier yielding ($\delta/\delta_{max} \approx 0.27$) the increase of rotation does not affect the horizontal movement of its top, but merely accumulates further plastic deformation at the failing section, as shown schematically in Fig. 8(c) for the case of decoupled system. As a result only the base of the pier moves to the left, leaving the top behind and leading to negative drift values. By contrast, for the coupled system fault dislocations are simultaneously imposed to the bedrock and the left abutment, as already mentioned, dragging the top of the pier further to the left and keeping the drift positive.

The distribution of bending moments across the deck, for imposed fault dislocation $\delta = 0.35\ \delta_{max}$, is presented in Fig. 9(a). Notably, the moment distribution has a discontinuity at the location of the pier. This jump is equal to the bending moment on top of the pier, as required for node equilibrium. Comparison of bending moments along the deck is presented in Fig. 9(b). The

evolution of settlement, rotation and horizontal displacement of footing (the output of step 1 of the decoupled model) is used as input at the base of the detailed model. As a result the discrepancies between the coupled and decoupled model, are caused by their discrepancies in terms of settlement and rotation of footing.

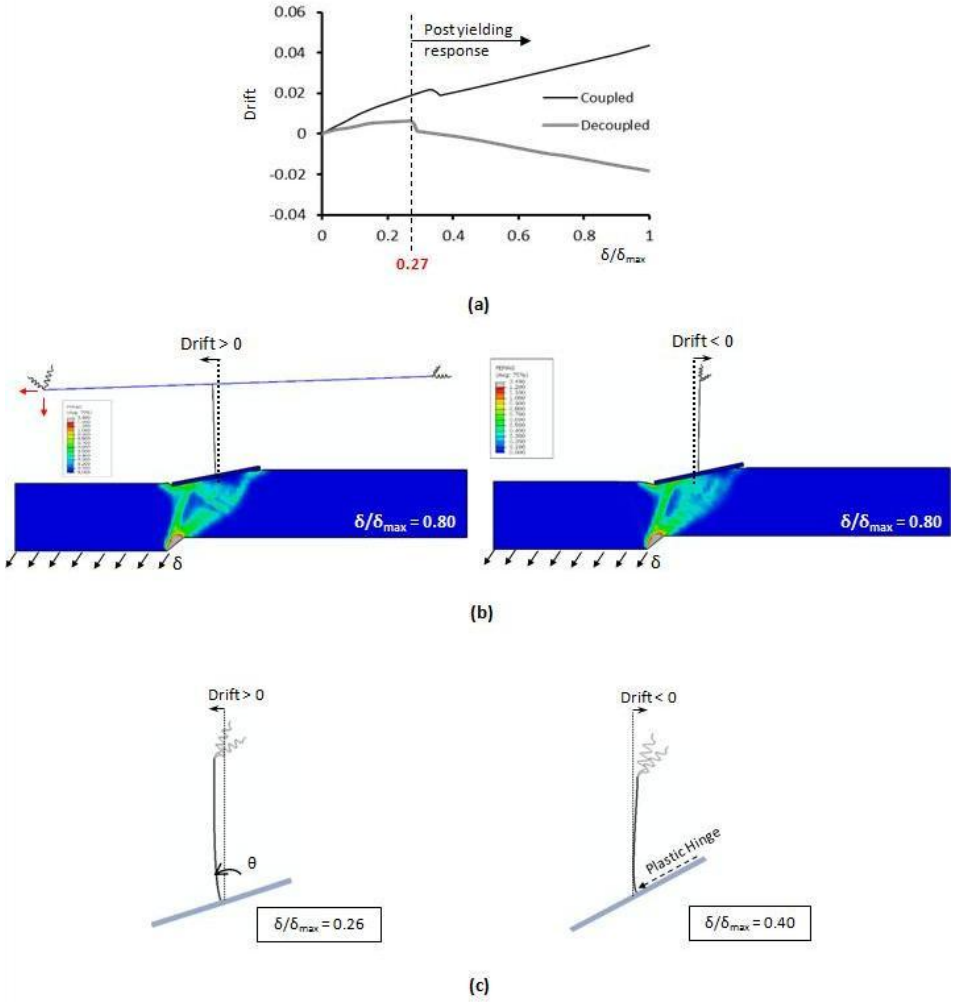

Figure 8. Bridge subjected to normal faulting analyzed ($\delta_{max} = -1.5$ m). Results are presented in terms of (a) drift ratio of the pier and (b) deformation snapshots superimposed with plastic deformation contours. (c) View of the deformed shape of decoupled system-pier, clarifying the differences of drift ratio before and after the development of plastic hinge (at instant $\delta/\delta_{max} = 0.27$)

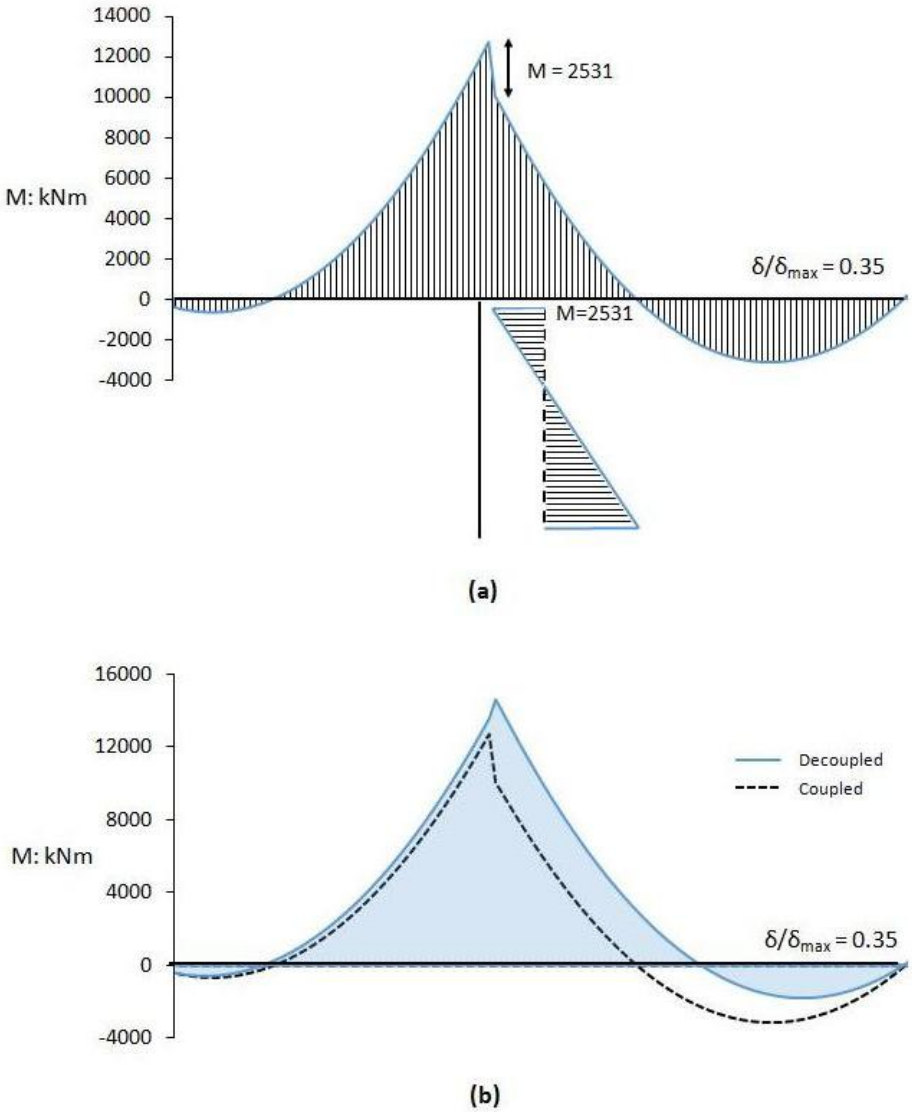

Figure 9. (a) Bending Moment distribution of the coupled system when subjected to normal faulting for $\delta/\delta_{max} = 0.35$ ($\delta_{max} = -1.5$ m); and (b) bending moment distribution along the bridge deck

6 RESULTS: BRIDGE SUBJECTED TO REVERSE FAULTING

Two reverse fault scenarios are examined in this section. First, the free-field rupture would have crossed the bridge–footing near its right corner (s/B=0.11), causing maximum displacements at the bottom of pier, while in the second scenario the free-field rupture would have crossed the bridge–footing near its

center (s/B=0.46). The two cases are schematically illustrated in Fig. 10. As it will be shown in the following, thanks to the presence of the foundation and the bridge, the fault rupture in both cases bifurcates and is diverted away from its free-field line, emerging well off the foundation area.

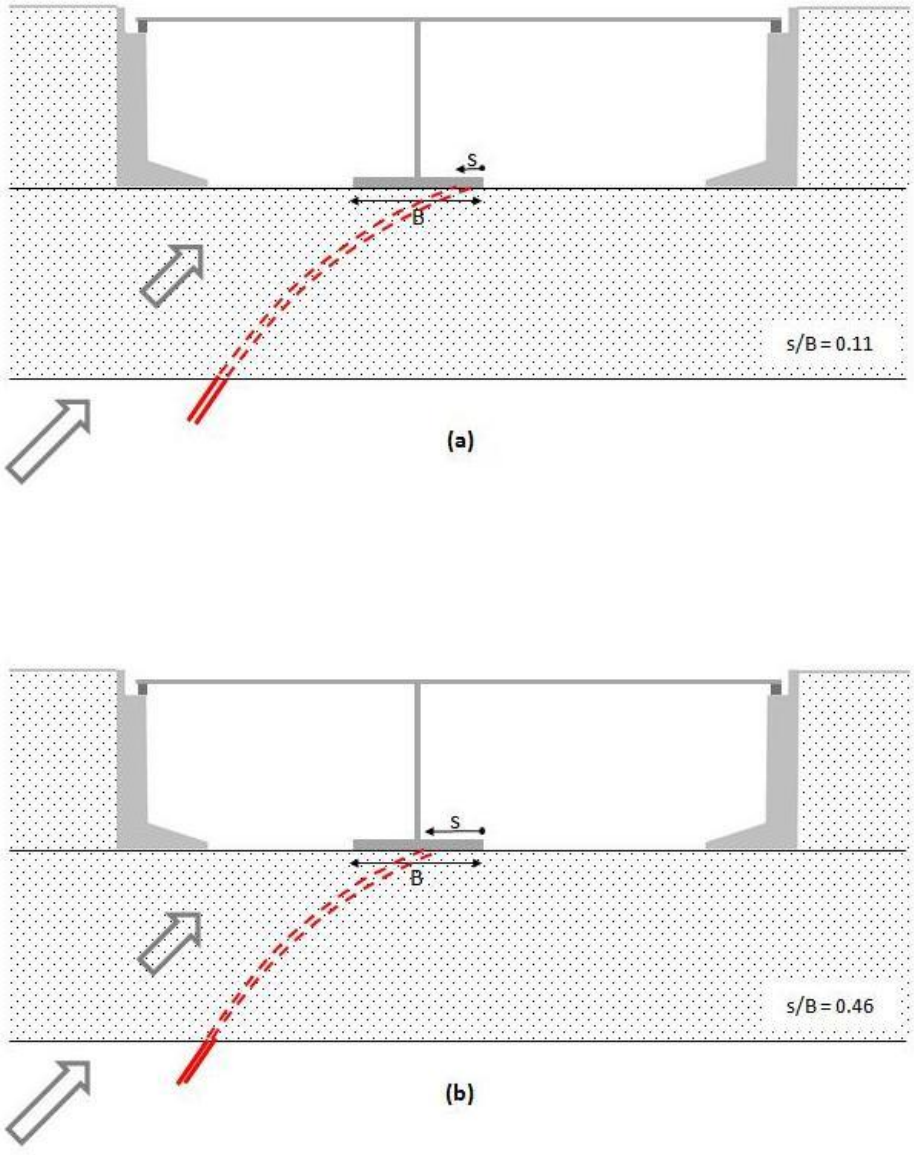

Figure 10. Bridge subjected to reverse faulting. *Free-field* rupture would have emerged: (a) at the location of the right corner of bridge footing (s/B = 0.11) and (b) at the location of the center of bridge footing (s/B = 0.46)

Location 1: s/B = 0.11

As evidenced by the plots of Fig. 11(a), and contrary to the trends observed in the normal faulting scenario, the footing settlement and rotation estimated by the coupled and decoupled methodology are quite different. Initially (i.e. for low values of faulting dislocations) both systems rotate clockwise, but soon after the decoupled system starts rotating backwards reaching at almost zero rotation at $\delta/\delta_{max} \approx 0.3$. At this point the bridge pier yields and the footing is practically enforced to follow the soil deformation (rotation to the right).

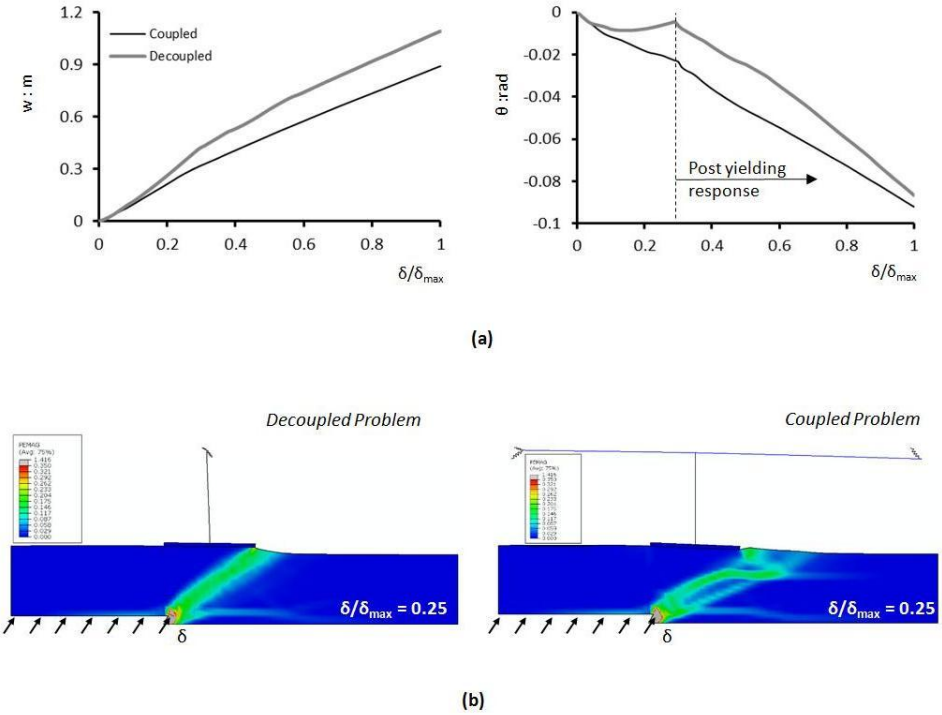

Figure 11. Bridge subjected to reverse faulting at s/B = 0.11 (δ_{max} = 1.5 m): (a) settlement (w) and rotation (θ) at the footing and (b) snapshots of two systems at fault dislocation level $\delta/\delta_{max} = 0.25$

With regard to the footing rotational response it would be reasonable to expect that the coupled system, experiencing much higher rotation, would fail first. Yet, this is not the case. Both methodologies predict bending failure at about the same fault dislocation, as shown in Fig. 12(a). At that particular δ the coupled system develops negative drift values, caused by displacement of the deck to-the-right. The latter induces positive curvature at the base of the pier that is partially cancelling the negative curvature produced by the footing rotation. A schematic representation of the aforementioned argument is shown in Fig. 12(c).

The distribution of bending moments across the deck of the bridge, for imposed fault dislocation (δ/δ_{max} = 0.10), is presented in Fig. 13(a), while Fig. 13(b) compares coupled and decoupled response. Notice that simplified decoupled methodology yields significantly higher bending moments (i.e. by a factor of 2), for reasons already explained.

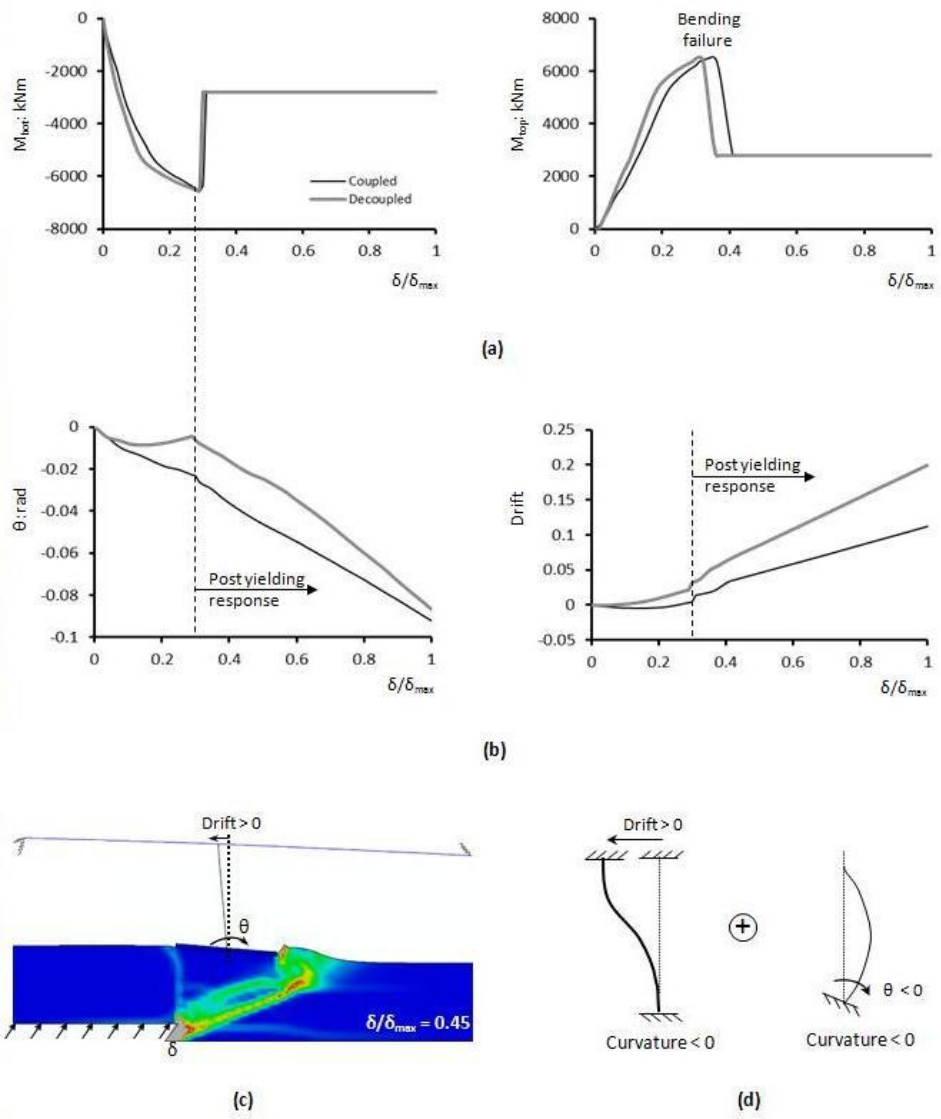

Figure 12. Bridge subjected to reverse faulting at s/B = 0.11 (δ_{max} = 1.5 m). Results are presented in terms of : (a) bending moments on the top (M_{top}) and bottom (M_{bot}) of the pier; and (b) rotation of footing (θ) and drift ratio of pier; (c) view of the deformed coupled system at δ/δ_{max} = 0.45; (d) kinematics responsible fro the bending stressing on the pier of the coupled system

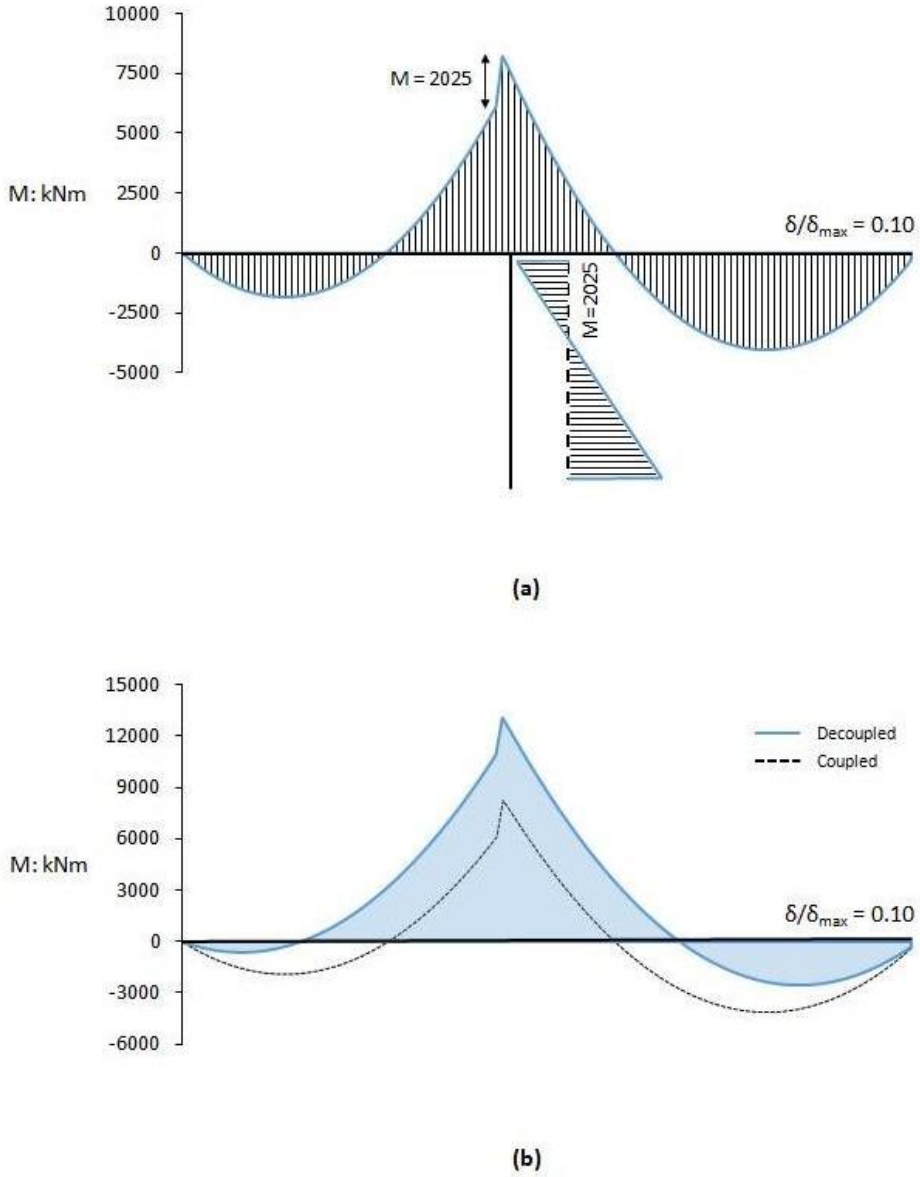

Figure 13. (a) Bending Stressing of the bridge (calculated by means of a coupled analysis) at reverse faulting s/B = 0.11, δ/δ_{max} = 0.10 (δ_{max} = 1.5 m); (b) bending moments along the bridge deck for both systems

Location 2: s/B = 0.46

Bending moments at the top and base of the two piers for the second investigated faulting scenario are portrayed in Fig. 14(a & d). Referring to

moments at pier base, the decoupled system is again yielding first, although the two systems experience identical footing rotations at that particular instant. Similarly with the previous explanation, the horizontal movement of the left abutment induces an opposite (favorable) curvature on the pier, preventing its bending failure.

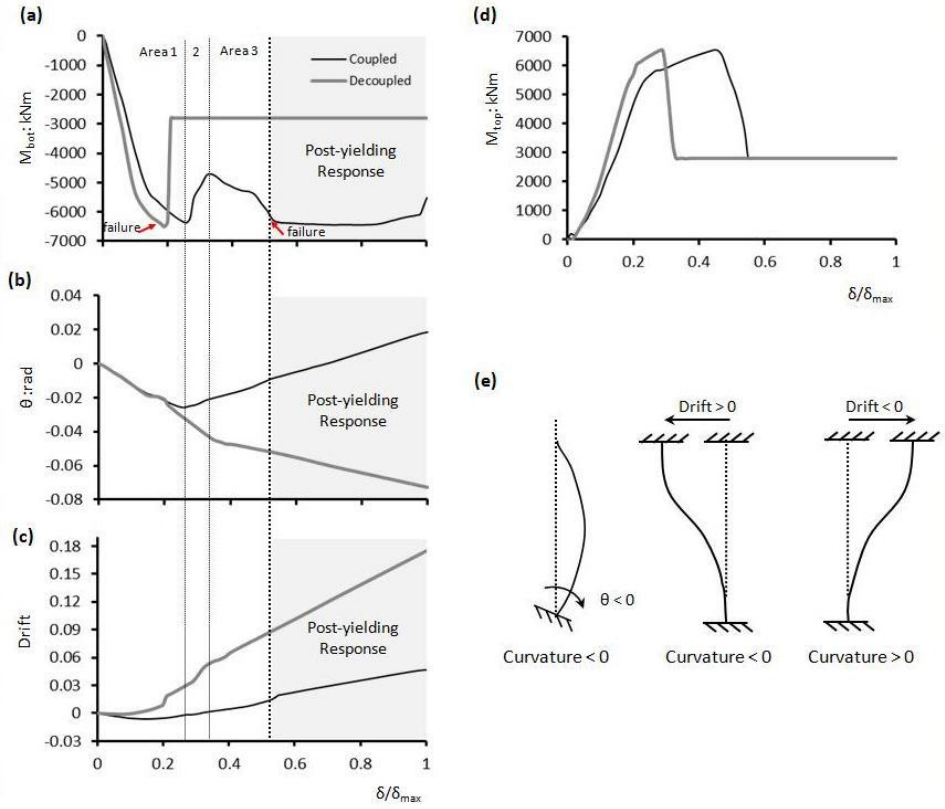

Figure 14. Bridge subjected to reverse faulting at s/B = 0.46 (δ_{max} = 1.5 m). Results are presented in terms of : (a) bending moments on the bottom (M_{bot}) of pier; (b) rotation (θ) of footing; (c) drift ratio of pier; and (d) bending moments on top (M_{top}) of the pier. (e) Deformation pattern nomenclature

Interestingly, the evolution of bending moment at the base of the coupled system follows an abnormal pattern: the moment peaks for fault offset $\delta/\delta_{max} \approx 0.24$ (Area 1), reduces for bedrock dislocations between $\delta/\delta_{max} \approx 0.24$ - 0.35 (Area 2) and continues increasing until it reaches the ultimate value $M_{max} \approx 6500$ kNm at $\delta/\delta_{max} \approx 0.5$ (Area 3). To explain this behavior, we separate the effects of the two competitive curvature-inducing mechanisms: the footing rotation and the horizontal dislocation of the abutment that provokes pier drift,

shown in Fig. 14(b & c). Initially (Area 1), the foundation rotates considerably under the action of the main fault-rupture, while the top of the pier practically remains still (almost zero drift). This footing rotation provokes negative curvature and thus negative bending actions on the pier. As the coupled system enters Area 2, the foundation starts rotating backwards, the curvature decreases and so does the bending moment (in absolute terms). In Area 3 the pier drift attains positive values that in turn generate negative curvature and negative moment. This continues until $\delta/\delta_{max} \approx 0.55$, the instant at which the pier ultimate capacity has been reached.

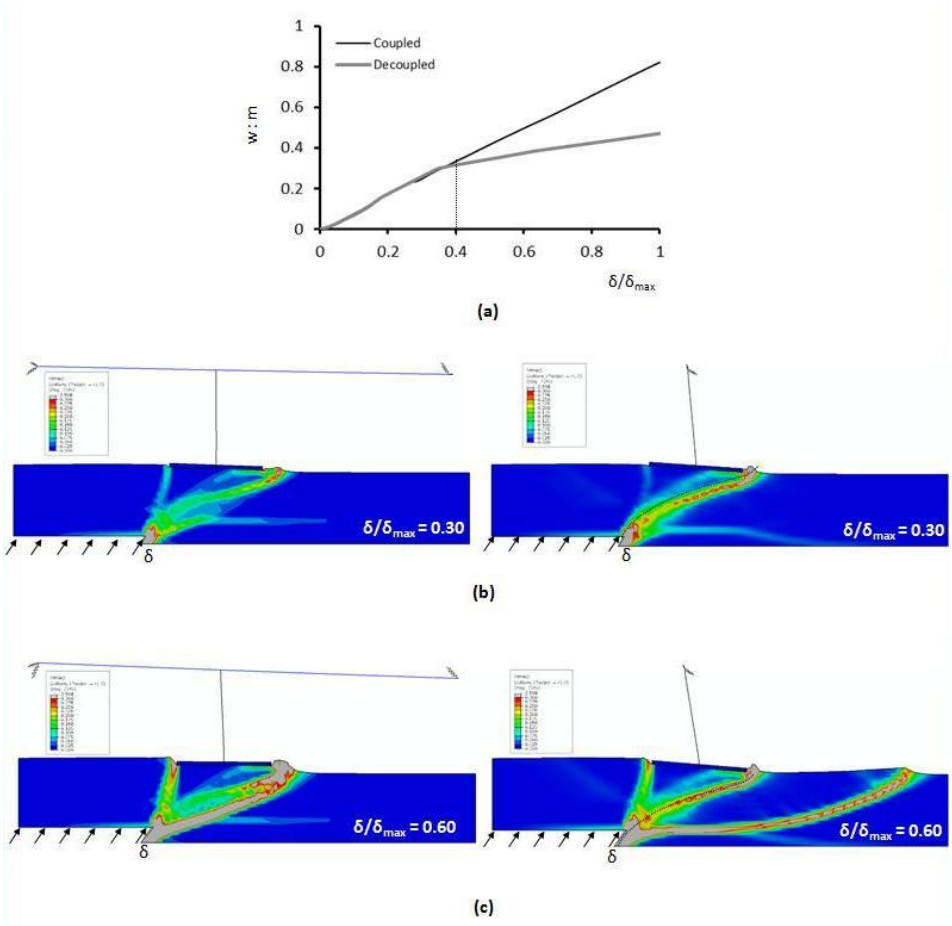

Figure 15. Bridge subjected to reverse faulting at s/B = 0.46 (δ_{max} = 1.5 m). (a) Footing settlement as derived by the coupled and the decoupled methodology. Deformation snapshots superimposed with plastic deformation contours for both systems at (b) δ/δ_{max} = 0.30 and (c) δ/δ_{max} = 0.60

For this faulting case, an interesting behavior (in terms of footing displacements) may also be observed. Up to imposed dislocation level of δ/δ_{max}

≈ 0.3, the two systems (coupled and decoupled) behave in a similar manner: both footings accumulate almost identical settlements and rotations. Beyond this point, the system response changes drastically. The footing of the coupled system starts rotating backwards (Fig. 16(a)), yet maintaining a constant rate of settlement accumulation, while the opposite holds for the footing of the de-coupled system.

To gain insight on this response, Fig. 15(b & c) presents a set of deformed snapshots at two distinctive bedrock dislocations ($\delta/\delta_{max} \approx 0.3$ and $\delta/\delta_{max} \approx 0.6$). The reader should observe the two ruptures interacting with the footing: a main rupture appearing near the footing right edge and a secondary rupture just behind the footing (evident for $\delta/\delta_{max} \approx 0.6$).

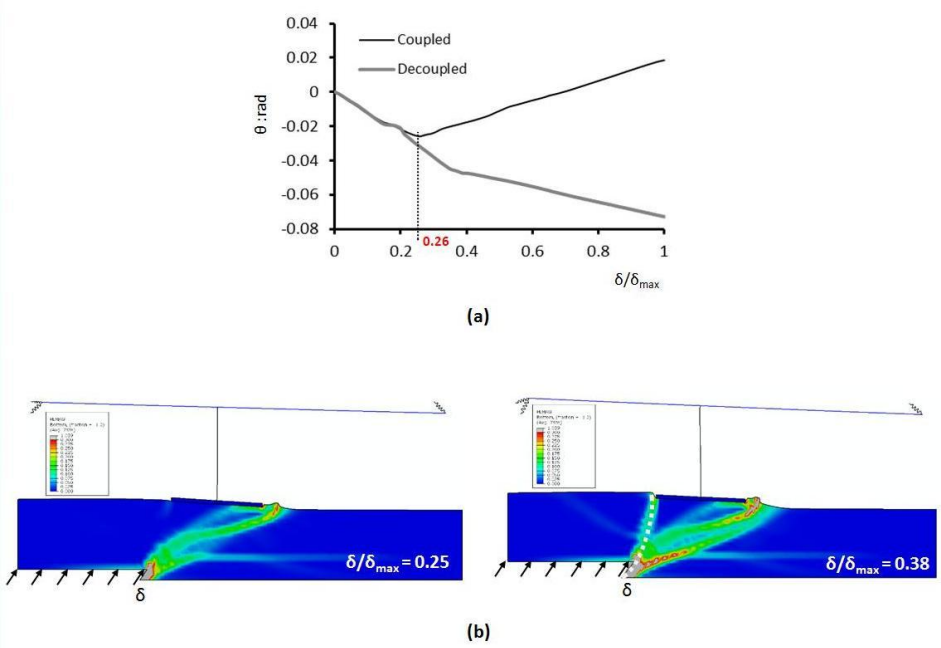

Figure 16. Bridge subjected to reverse faulting at s/B = 0.46 (δ_{max} = 1.5 m): (a) foundation rotation (θ) and (b) snapshots of the coupled system at two distinctive bedrock dislocations δ/δ_{max} = 0.25 and 0.38

Clearly, the main rupture dominates the response for bedrock dislocations lower than δ/δ_{max} = 0.30. Yet for higher dislocation values the pattern gets more complex. On the coupled system plastic strains keep accumulating along the main rupture, while in the decoupled system the secondary rupture is gaining ground. [Note that the intensity of plastic deformations in the main rupture remains practically unchanged from δ/δ_{max} = 0.30 to 0.60]. The latter forms a graben type settlement beneath the footing (of the coupled system) which

restrains any additional clockwise foundation rotation (the footing tends to rotate in the opposite direction).
The distribution of bending moments across the deck of bridge for a fault dislocation δ/δ_{max} = 0.20 is presented in Fig. 17(a), while in Fig. 17(b) a comparison between the coupled and decoupled system in terms of bending moments across the deck (for the same level of faulting) is presented. The response of two systems, for the exact fault level, is identical.

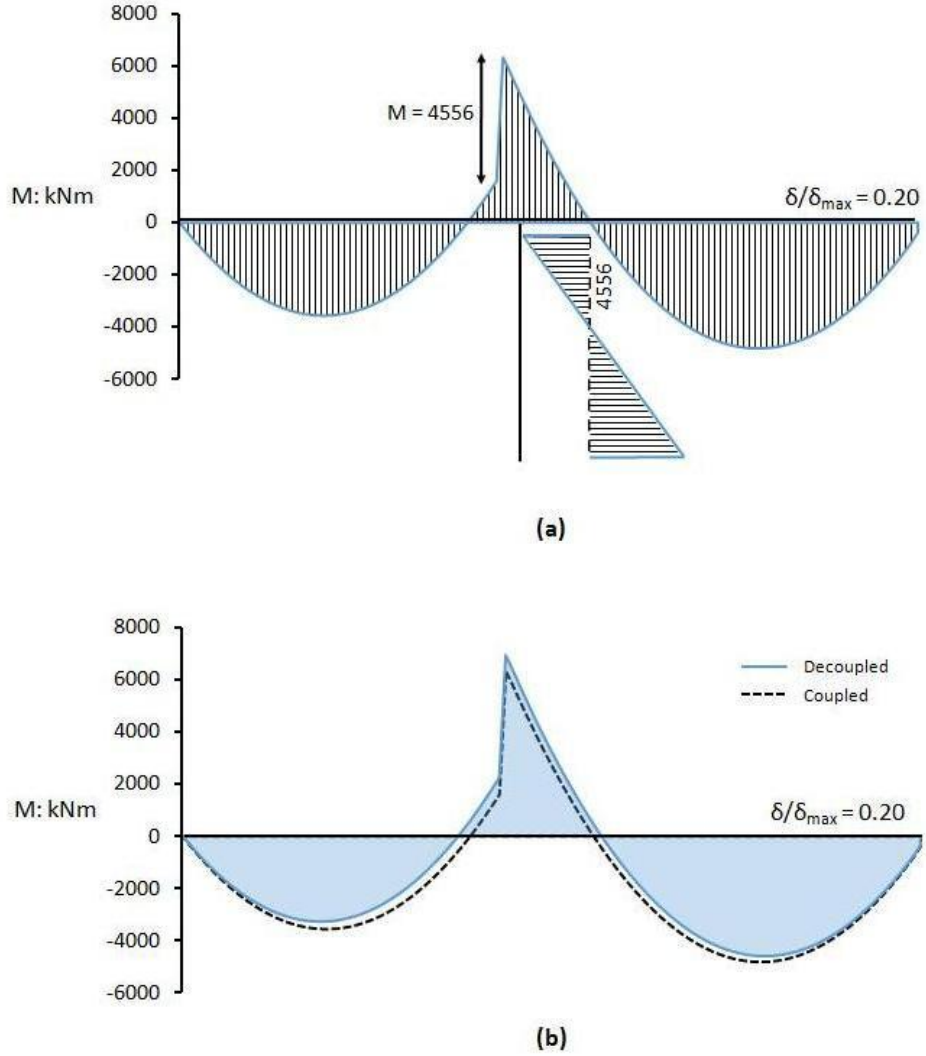

Figure 17. (a) Bending Stressing of the bridge (calculated by means of a coupled analysis) at reverse faulting s/B = 0.46, δ/δ_{max} = 0.20 (δ_{max} = 1.5 m); and (b) bending moments along the bridge deck for both systems

8 CONCLUSIONS

This paper presents a numerical methodology to analyze the response of bridges against large tectonic deformation accounting in a realistic way of the coupling of the response of the foundation with the superstructure. The numerical results have been systematically compared to those produced by applying the simplified decoupled methodology suggested by *Anastasopoulos et al. 2008.* The following conclusions are derived:

1. The design of bridges against tectonic deformation is quite feasible with proper design. The decoupled method of analysis presented by *Anastasopoulos et al. 2008* may form the basis for future Code provisions and requirements on the subject.
2. This efficiency of the decoupled methodology depends on the accurate prediction of settlements and rotations at the bridge footings.
3. The rupture path is strongly affected by the presence of the superstructure and its foundations. The emerging fault rupture is not only diverted, but may also develop bifurcation and diffusion.
4. The bridge system with simple movable supports on its abutments leads to low pier bending moments. Therefore it is vital (in the forthcoming scaled experiments) to correctly model the abutment stiffness in the laboratory set-up, in order to correctly simulate the bridge-fault interaction problem.

The results of the experimental study will be given in a forthcoming companion paper, which will evaluate the performance of our numerical modeling.

ACKNOWLEDGEMENT

The presented research has been financially supported by the Greek State Scholarship Foundation (IKY Fellowships of Excellence for Postgraduate Studies in Greece – Siemens Program).

REFERENCES

[1] Anastasopoulos I, Gazetas G, Bransby MF, Davies MCR, El NahasA(2007) Fault rupture propagation through sand: finite element analysis and validation through centrifuge experiments. *J Geotech Geoenviron Eng* 133(8):943–958

[2] Anastasopoulos I, Gazetas G, Drosos V, Georgarakos T, Kourkoulis R (2008) Design of bridges against large tectonic deformation. *Earthq Eng Eng Vib* 7:345–368

[3] Anastasopoulos I, Gazetas G, Bransby MF, Davies MCR, El Nahas A (2009) Normal fault rupture interaction with strip foundations. *J Geotech Geoenviron Eng* 135(3):359–370

[4] Anastasopoulos I, Georgarakos T, Georgiannou V, Drosos V, Kourkoulis R (2010) Seismic performance of bar-mat reinforced-soil retaining wall: shaking table testing versus numerical analysis with modified kinematic hardening constitutive model. *Soil Dyn Earthq Eng* 30(10):1089–1105

[5] Bolton MD (1986) The strength and dilatancy of sands. *Geotechnique* 36(1):65–78

[6] Bransby MF, Davies MCR, El Nahas A, Nagaoka S (2008) Centrifuge modelling of normal fault-foundation interaction. *Bull Earthq Eng* 6(4):585–605

[7] Bray JD, Seed RB, Cluff LS, Seed HB (1994) Analysis of earthquake fault rupture

propagation through cohesive soil. *J Geotech Eng* 120(3):562–580
[8] Bray JD, Seed RB, Cluff LS, Seed HB (1994) Earthquake fault rupture propagation through soil. *J Geotech Eng* 120(3):543–561
[9] Bray JD (2001) Developing mitigation measures for the hazards associated with earthquake surface fault rupture. *Workshop on Seismic fault-induced failures—Possible Remedies for Damage to Urban Facilities*, Japan Society for the Promotion of Sciences, 55–79
[10] Bray JD (2009) Designing buildings to accommodate earthquake surface fault rupture, improving the seismic performance of existing and other structures. ASCE Specialty Publication, Reston Virginia, pp 1269–1280
[11] Fadaee M, Anastasopoulos I, Gazetas G, Jafari MK, Kamalian M (2013) Soil bentonite wall protects foundation from thrust faulting: analyses and experiment. *Earthq Eng Eng Vib* 12(3):473–486
[12] Gazetas G, Pecker A, Faccioli E, Paolucci R, Anastasopoulos I (2008) Design recommendations for fault–foundation interaction. *Bull Earthq Eng* 6(4):677–687
[13] Gazetas G, Zarzouras O, Drosos V, Anastasopoulos I (2015) Bridge-Pier-Caisson foundations subjected to normal and thrust faulting: physical experiments versus numerical analysis. *Meccanica* (2015) 50:341–354
[14] Loli M, Anastasopoulos I, Bransby MF, Waqas A, Gazetas G (2011) Caisson foundations subjected to reverse fault rupture: centrifuge testing and numerical analysis. *J Geotech Geoenviron Eng* 137(10):914–925
[15] Loukidis D, Bouckovalas G, Papadimitriou AG (2009) Analysis of fault rupture propagation through uniform soil cover. *Soil Dyn Earthq Eng* 29(11–12):1389–1404
[16] Muir Wood D (2004) *Geotechnical modelling*. Spon Press, London and New York
[17] Oettle NK, Bray JD (2013) Geotechnical mitigation strategies for earthquake surface fault rupture. *Geotech Geoenviron Eng* 139(11):1864–1874
[18] Paolucci R, Yilmaz MT (2008) Simplified theoretical approaches to earthquake fault rupture–shallow foundation interaction. *Bull Earthq Eng* 6(4):629–644